Capillary meniscus interaction between a microparticle and a wall

V.N. Paunov[a], P.A. Kralchevsky[a], N.D. Denkov[a], I.B. Ivanov[a] and K. Nagayama[b]

[a]*Laboratory of Thermodynamics and Physico-Chemical Hydrodynamics, University of Sofia, Faculty of Chemistry, Sofia 1126, Bulgaria*
[b]*Nagayama Protein Array Project, ERATO, JRDC, 18-1 Higashiarai, Tsukuba 305, Japan*

Abstract

An analytical expression for the shape of the capillary menis.. s formed around a vertical cylinder or spherical particle near a vertical wall is derived by using the method of matched asymptotic expansions. The forces of capillary interaction between the particle (cylinder) and the wall are calculated. The resulting expressions are valid when the distance between the particle (cylinder) and the wall, as well as the particle radius, are much smaller than the capillary length. This range corresponds to colloidal and micron-size particles. The theory predicts attraction between such a particle and the wall. The results can be useful for a better understanding of processes such as surface coagulation and two-dimensional ordering of colloidal particles or protein molecules attached to a fluid interface.

1. Introduction

The deformation of a liquid–fluid interface due to trapped small particles gives rise to capillary forces exerted on the particles. Usually these forces are attractive and lead to formation of clusters. Such effects were observed long ago and are utilized in some extraction and separation flotation processes (see for example Refs [1,2]). The capillary meniscus interactions were studied experimentally by Hinsch [3] and Camoin et al. [4]. These forces can be among the main factors leading to formation of two-dimensional clusters and ordered structures observed with micron-size particles [5–7] as well as with protein molecules [8–10].

Despite the well-established importance of the capillary meniscus forces, there are only a few theo-

retical works devoted to them. Nicolson [11] derived an analytical expression for the capillary force between two floating bubbles by using the superposition approximation to solve the Laplace equation of capillarity. A similar approximate method was applied by Chan et al. [12] to floating spheres and horizontal cylinders. For the latter case alternative approaches were proposed by Gifford and Scriven [13] and by Fortes [14]. The theoretical works [11–14] are based on solutions of the Laplace equation for capillary menisci of translational or rotational symmetry, where the Laplace equation reduces to an ordinary differential equation.

A recent development in this field is the analytical solution of the Laplace partial differential equation in bipolar coordinates proposed in Refs [15,16] for the case of small particles and small meniscus slope. This solution provides expressions for calculating the capillary meniscus force between two vertical cylinders, between two spheres par-

tially immersed in a liquid layer, and between a vertical cylinder and a sphere. It was established that the capillary meniscus forces are comparatively long range and the energy of interaction is much larger than the thermal energy kT even for submicron particles.

Since the above theoretical results are valid for particles of small radii (not larger than about 100 µm), they cannot be applied to describe the capillary interaction between a particle and a larger aggregate or between a particle and a vertical wall. This problem is considered in the present paper. An asymptotic expression for calculating the shape of the capillary meniscus around a vertical cylinder near a wall is derived in the next section. Equations for the shape of the two contact lines are also obtained. Then expressions for the capillary meniscus forces exerted on the cylinder and on the wall are derived. The results also allow calculation of the capillary interaction between a wall and a spherical particle which is partially immersed in a liquid layer. The analytical expressions are illustrated with three-dimensional graphs of the meniscus shape and plots of the capillary forces vs distance between the particle and the wall.

In general, the capillary force exerted on a particle is an integral effect of the action of the hydrostatic pressure through the wet surface and of the interfacial tension along the three-phase contact line. We mention in advance that the capillary forces due to hydrostatic pressure exerted on the particle and on the wall are not of equal magnitude. However, it turns out that the horizontal projections of the total (hydrostatic pressure plus interfacial tension) capillary forces exerted on the particle and on the wall have equal magnitude and opposite directions, i.e. they obey a counterpart of Newton's third law; this is proved in Appendix A.

2. Shape of the capillary meniscus

2.1 Basic equations

Let us consider the capillary meniscus formed around a vertical circular cylinder, whose axis is

separated at a distance s from a flat vertical plate (Fig. 1). When the cylinder is situated far away from the vertical plate ($s \to \infty$), the menisci on the right and on the left from the plate are similar; their shape has already been described theoretically [17]. Our aim below is to derive an expression for the shape of the meniscus on the right from the plate for finite values of s.

The interface between the two fluid phases I and II is supposed to be flat and horizontal far away from the cylinder and the wall. We choose the coordinate plane xy to coincide with this horizontal surface. Let

$$z = \zeta(x, y) \qquad (2.1)$$

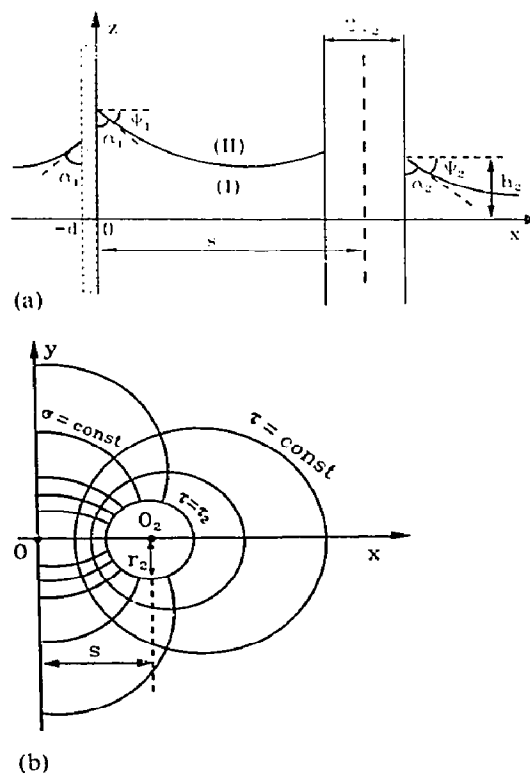be the equation describing the shape of the inter-

Fig. 1. Sketch of (a) the capillary meniscus formed around a cylinder of radius r_2 situated at a distance s from a flat vertical wall, and (b) the bipolar coordinates used in the plane xy (α_1 and α_2 are the three-phase contact angles at the wall and cylinder surface, respectively; h_2 is the elevation of the cylinder contact line above the flat interface at $x \to \infty$; the lines $x = 0$ and $\tau = \tau_2 = $ constant are the projections of the wall and cylinder in the plane xy).

face. The function ζ can be both positive and negative, depending on the values of the three-phase contact angles α_1 and α_2 formed at the wall and cylinder surface (see Fig. 1(a) and Ref. [17]). Here and subsequently the parameters connected with the wall and the cylinder are denoted by indices 1 and 2 respectively.

The geometry of the system suggests the introduction of bipolar coordinates in the plane xy (see for example Ref. [18] and Fig. 1(b)):

$$x = \frac{a \sinh \tau}{\cosh \tau - \cos \sigma} \qquad y = \frac{a \sin \sigma}{\cosh \tau - \cos \sigma} \qquad (2.2)$$

$$-\pi \leqslant \sigma \leqslant \pi \qquad 0 \leqslant \tau < \infty$$

Each line $\tau = $ constant is a circumference [18]:

$$(x - a \coth \tau)^2 + y^2 = \frac{a^2}{\sinh^2 \tau} \qquad (2.3)$$

If the surface of the wall coincides with the coordinate plane yz and $\tau = \tau_2 = $ constant is the equation of the cylinder surface, then in accordance with Eqn (2.3) one finds

$$s = a \coth \tau_2 \qquad (2.4)$$

$$r_2 = a/\sinh \tau_2 \qquad (2.5)$$

where r_2 is the radius of the cylinder. From Eqns (2.4) and (2.5) one determines the parameter a:

$$a = \sqrt{s^2 - r_2^2} \qquad (2.6)$$

We restrict our consideration to the case where the slope of the meniscus surface is small, i.e.

$$\left(\frac{\partial \zeta}{\partial x}\right)^2 \ll 1 \qquad \text{and} \qquad \left(\frac{\partial \zeta}{\partial y}\right)^2 \ll 1 \qquad (2.7)$$

Under this restriction the Laplace equation of capillarity, which determines the meniscus shape, reads [15,17]

$$\frac{\partial^2 \zeta}{\partial x^2} + \frac{\partial^2 \zeta}{\partial y^2} = q^2 \zeta \qquad (2.8)$$

where

$$q^2 = \Delta \rho g / \gamma \qquad \Delta \rho = \rho_1 - \rho_{\text{II}} \qquad (2.9)$$

ρ_1 and ρ_{II} are the mass densities of phases I and II; γ is the interfacial tension; g is the acceleration due to gravity.

In bipolar coordinates Eqn (2.8) has the form (see for example Ref. [18]):

$$(\cosh \tau - \cos \sigma)^2 \left(\frac{\partial^2 \zeta}{\partial \sigma^2} + \frac{\partial^2 \zeta}{\partial \tau^2}\right) = (qa)^2 \zeta(\sigma, \tau) \qquad (2.10)$$

Usually $q \approx 5 \, \text{cm}^{-1}$; then for small values of a ($a \leqslant 100 \, \mu\text{m}$) one has $(qa)^2 \leqslant 2.5 \cdot 10^{-3}$. If such is the case, Eqn (2.10) contains a small parameter and its solution can be found in the form of an asymptotic expansion.

One sees that however small $(qa)^2$ may be, the right-hand side of Eqn (2.10) can be comparable with the left-hand side when σ and τ tend simultaneously to zero. That is why in keeping with the method of the matched asymptotic expansions (see for example Ref. [19]) we consider an inner and an outer region:

inner region (close to the cylinder):

$$(\cosh \tau - \cos \sigma)^2 \gg (qa)^2$$

outer region (far from the cylinder):

$$(\cosh \tau - \cos \sigma)^2 \leqslant (qa)^2$$

The solutions of Eqn (2.10) in these two regions are considered separately below.

2.2 Inner region

In the inner region, Eqn (2.10) reduces to

$$\frac{\partial^2 \zeta}{\partial \sigma^2} + \frac{\partial^2 \zeta}{\partial \tau^2} = 0 \qquad (2.11)$$

(In fact Eqn (2.11) determines the zeroth-order solution for $\zeta(\sigma,\tau)$.) One can seek the solution of Eqn (2.11) in the form of a Fourier series:

$$\zeta(\sigma,\tau) = C_0 + B_0 \tau + \sum_{n=1}^{\infty} B_n$$

$$\times \exp(-n\tau) \cos n\sigma \qquad \tau \geqslant 0 \qquad (2.12)$$

The integration constants B_n, where $n = 0, 1, 2, \ldots$, are determined from the boundary condition for constancy of the contact angle at the cylinder surface:

$$-e_\tau \cdot n|_{\tau = \tau_2} = \cos \alpha_2 = \text{constant} \qquad (2.13)$$

where e_τ is the running unit tangent to the τ lines (obviously e_τ is normal to the cylinder surface) and n is the running unit normal to the liquid interface. By using the methods of differential geometry (see for example Ref. [20]) along with the restriction for small slope, Eqn (2.7), one can transform Eqn (2.13) to read

$$\left.\frac{\partial \zeta}{\partial \tau}\right|_{\tau = \tau_2} = \frac{a \sin \psi_2}{\cosh \tau_2 - \cos \sigma} \qquad (2.14)$$

where angle ψ_2 characterizes the meniscus slope at the contact line (see also Fig. 1):

$$\sin \psi_2 = \cos \alpha_2 \qquad (2.15)$$

By expanding the right-hand side of Eqn (2.14) in a Fourier series one obtains

$$\left.\frac{\partial \zeta}{\partial \tau}\right|_{\tau = \tau_2} = r_2 \sin \psi_2$$
$$\times \left(1 + 2 \sum_{n=1}^{\infty} \exp(-n\tau_2) \cos n\sigma\right) \qquad (2.16)$$

where Eqn (2.5) is also used. A comparison between Eqns (2.12) and (2.16) yields

$$B_0 = r_2 \sin \psi_2 \qquad B_n = -\frac{2}{n} r_2 \sin \psi_2$$
$$n = 1, 2, \ldots \qquad (2.17)$$

By substituting from Eqn (2.17) into Eqn (2.12) one finds the sought for solution of the Laplace equation in the inner region:

$$\zeta^{in}(\sigma, \tau) = C_0 + r_2 \sin \psi_2 \ln(2 \cosh \tau - 2 \cos \sigma) \qquad (2.18)$$

Here we have used the identity

$$\tau - 2 \sum_{n=1}^{\infty} \frac{1}{n} \exp(-n\tau) \cos n\sigma$$
$$= \ln(2 \cosh \tau - 2 \cos \sigma) \qquad (2.19)$$

By differentiating Eqn (2.18) one can show that

$$\left.\frac{\partial \zeta^{in}}{\partial \tau}\right|_{\tau = 0} = 0 \qquad (2.20)$$

Besides, by using the expressions

$$\tau|_{y=0} = \ln \left|\frac{x+a}{x-a}\right| = 2 \left[\frac{a}{x} + O\left(\frac{a^3}{x^3}\right)\right] \qquad (2.21)$$

and

$$\left.\left(\sin^2 \frac{\sigma}{2}\right)\right|_{x=0} = [1 + (y^2/a^2)]^{-1} \qquad (2.22)$$

stemming from Eqn (2.2), from Eqn (2.18) one can derive the asymptotics of ζ^{in} along the x and y axes:

$$\zeta^{in}(0,\tau) = C_0 + r_2 \sin \psi_2 \left[2 \ln\left(\frac{2a}{x}\right)\right.$$
$$\left. + O\left(\frac{a^2}{x^2}\right)\right] \qquad x \gg 1 \qquad (2.23)$$

$$\zeta^{in}(\sigma,0) = C_0 + r_2 \sin \psi_2 \left[2 \ln\left(\frac{2a}{y}\right)\right.$$
$$\left. + O\left(\frac{a^2}{y^2}\right)\right] \qquad y \gg 1 \qquad (2.24)$$

The comparison between Eqns (2.23) and (2.24) shows that the outer asymptotics of the inner solution can be written in the form

$$(\zeta^{in})^{out} = C_0 + r_2 \sin \psi_2 \left[2 \ln\left(\frac{2a}{r}\right) + O\left(\frac{a^2}{r^2}\right)\right] \qquad (2.25)$$

where

$$r = \sqrt{x^2 + y^2} \qquad (2.26)$$

The constant C_0 is determined by matching the inner with the outer solution.

2.3 Outer solution and procedure of matching

We seek the solution of Eqn (2.8) in the outer region in the form

$$\zeta^{out}(x, y) = E \exp(-qx) + GK_0(qr) \qquad x \geqslant 0 \tag{2.27}$$

where E and G are integration constants, K_0 is a modified Bessel function (see for example Ref. [18]). The first term on the right-hand side of Eqn (2.27) describes the shape of the meniscus due to a single vertical wall, whereas the second term describes the meniscus shape around a single vertical cylinder. One can easily check that the function $\zeta = \zeta^{out}(x, y)$ given by Eqn (2.27), satisfies both Eqn (2.8) and the boundary condition

$$\lim_{x \to \infty} \zeta(x, y) = 0 \tag{2.28}$$

From the condition for constancy of the contact angle at the wall

$$\left.\frac{\partial \zeta}{\partial x}\right|_{x=0} \approx -\frac{1}{\tan \alpha_1} = -\tan \psi_1 \tag{2.29}$$

(cf. Eqn (2.7) and Fig. 1) one determines constant E in Eqn (2.?)

$$E = \left(\frac{1}{q}\right)\left(-\frac{1}{\tan \alpha_1}\right) = \frac{1}{q} \tan \psi_1 \tag{2.30}$$

where α_1 is the contact angle at the wall measured through phase I. The constant G, as well as the constant C_0 in Eqn (2.18), is determined by means of the condition for matching the outer and inner solutions [19]

$$(\zeta^{in})^{out} = (\zeta^{out})^{in} \tag{2.31}$$

By expanding Eqn (2.27) in series for small r one obtains

$$(\zeta^{out})^{in} = E - G \ln(\gamma_e/2) - G \ln(qr) + O(qx) \tag{2.32}$$

where $\gamma_e = 1.781\,072\,418 \ldots$, and $\ln \gamma_e$ is the Euler–Masceroni number (see for example Ref. [18]). A substitution from Eqns (2.25) and (2.32) into Eqn (2.31), along with Eqn (2.30), yields

$$G = 2r_2 \sin \psi_2$$

$$C_0 = \frac{1}{q} \tan \psi_1 - 2r_2 \sin \psi_2 \ln(\gamma_e q a) \tag{2.33}$$

The compound solution, which is uniformly valid both in the outer and the inner region is [19]

$$\zeta = \zeta^{in} + \zeta^{out} - (\zeta^{in})^{out} \tag{2.34}$$

Then from Eqns (2.18), (2.25), (2.27), (2.33) and (2.34) one derives an explicit expression for the compound solution:

$$\zeta(\sigma,\tau) = \frac{1}{q} \tan \psi_1 \exp(-qx) + r_2 \sin \psi_2$$
$$\times \left[2K_0(qr) + 2 \ln \frac{r}{2a} + \ln(2 \cosh \tau - 2 \cos \sigma) \right] \qquad x \geqslant 0 \tag{2.35}$$

Equation (2.35), together with Eqns (2.2) and (2.26), allows calculation of the shape of the capillary meniscus. One can check that Eqn (2.35) satisfies all necessary boundary conditions, Eqns (2.14), (2.28) and (2.29). Besides, the terms in Eqn (2.35) containing logarithmic divergences cancel each other, and the whole expression is regular for $r \to 0$ and $r \to \infty$.

It should be noted that Eqn (2.35) represents a zeroth-order compound asymptotic solution for the meniscus shape, which is valid for $(qa)^2 \ll 1$ and for small meniscus slope (see Eqn (2.7)). These conditions are satisfied very well with small particles (see below), so Eqn (2.35) can be used to describe the capillary interactions governing various processes of surface aggregation of colloidal particles near a wall.

Figure 2 represents illustrative examples of the shape of the meniscus surface calculated by means of Eqn (2.35) for two different cases. In Fig. 2(a) the slope angles at the two contact lines have the same sign: $\psi_1 = 0.5°$, $\psi_2 = 5°$, whereas in Fig. 2(b) they have opposite signs: $\psi_1 = 0.5°$, $\psi_2 = -5°$. In both cases $s = 4 \mu m$, $r_2 = 1 \mu m$ and $q^{-1} = 0.2$ cm. The holes in the surfaces depicted in Figs 2(a) and 2(b) correspond to the places where the respective cylinders pierce the interface. The periphery of the holes is not smooth because of the square coordinate network used in the computer program. (The real smooth contact line on the cylinder is not
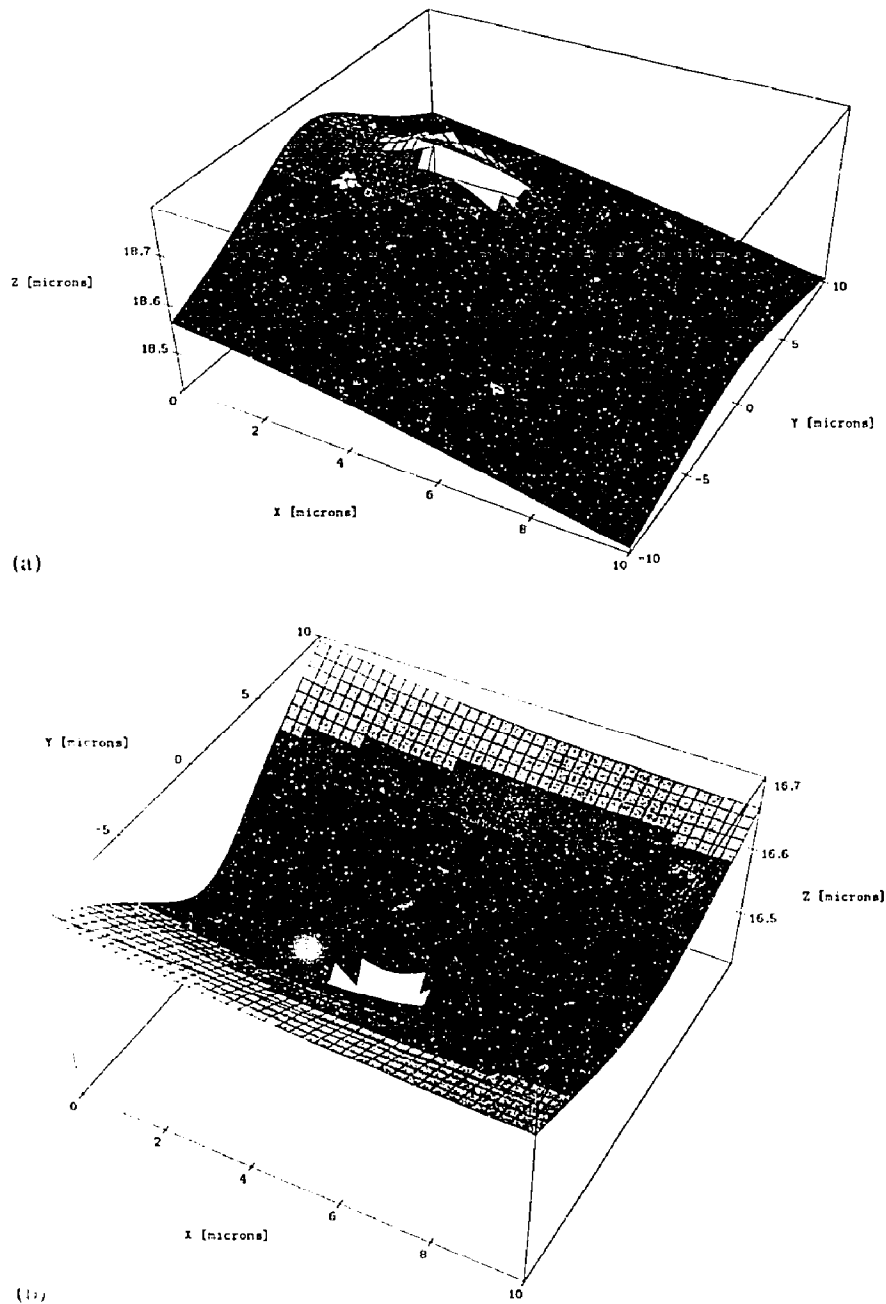
Fig. 2. Shape of the capillary meniscus surface calculated from Eqn (2.35): (a) $\psi_1 = 0.5$, $\psi_2 = 5$; (b) $\psi_1 = 0.5$, $\psi_2 = -5$. In both cases $s = 4$ μm, $r_2 = 1$ μm, $q^{-1} = 0.2$ cm.

shown in the figures because of the resolution of the plotting program.) One sees that in Fig. 2(a) the meniscus between the wall and cylinder has a saddle-like shape, which is not the case in Fig. 2(b). Nevertheless it is shown below that in both cases

the capillary forces correspond to attraction between the cylinder and the wall.

In the case where $\psi_1 = 0$ (i.e. the contact angle at the wall is $\alpha_1 = 90°$), Eqn (2.35) is equivalent to Eqns (2.49)–(2.52) in Ref. [15]. Hence in this case

the meniscus between the cylinder and the wall has the same shape as the meniscus between two similar cylinders of radius r_2, each of them being the mirror image of the other one with respect to the wall surface. That is why in such a case the capillary interaction between the cylinder and the wall is the same as between the cylinder and its mirror image. In this respect there is some analogy with the image forces in electrostatics.

3. Shape of the three-phase contact lines

The shape of the contact line at the vertical wall can be determined by setting $x = 0$ ($\tau = 0$, $r = y$) in Eqn (2.35). In accordance with Eqn (2.22) one obtains

$$\zeta_1(y) \equiv \zeta|_{x=0} = \frac{1}{q} \tan \psi_1 + r_2 \sin \psi_2$$

$$\times \left[2K_0(q|y|) - \ln\left(1 + \frac{a^2}{y^2}\right) \right] \quad (3.1)$$

For large y, Eqn (3.1) yields

$$\zeta_1(y) \to \zeta_r = \frac{1}{q} \tan \psi_1 = \text{constant} \qquad |y| \gg a, q^{-1}$$

$$(3.2)$$

In fact the constant ζ_r represents the elevation of the contact line at a single vertical wall. At $y = 0$ the contact line exhibits a maximum elevation:

$$\zeta_1(0) = \frac{1}{q} \tan \psi_1 - 2r_2 \sin \psi_2 \ln(\gamma_c q a/2) \quad (3.3)$$

(Note that $(qa)^2 \ll 1$, so the logarithm in Eqn (3.3) is negative.) Figure 3 represents the shape of the contact line at the wall for different vaues of qa. One sees that the elevation of the contact line increases when the distance between the cylinder and the wall decreases (qa decreases (cf. Eqn (2.6) and Fig. 1)). If $\psi_2 < 0$, the elevation $\zeta_1 - \zeta_\alpha$ will also have a negative sign. The area below each curve in Fig. 3 is proportional to the change in the
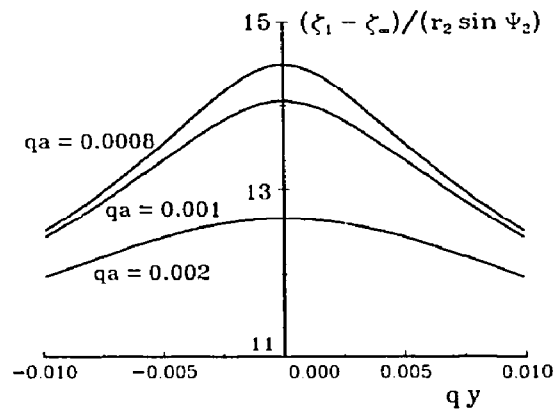

Fig. 3. Shape of the three-phase contact line on the wall, calculated from Eqns (3.1) and (3.2) for three values of qa.

wet area due to the presence of the cylinder:

$$\Delta A = \int_{-\infty}^{\infty} [\zeta_1(y) - \zeta_r] \, dy = 2\pi r_2 \sin \psi_2(q^{-1} - a)$$

$$(3.4)$$

Here we have used Eqns (3.1) and (3.2).

The shape of the contact line at the surface of the vertical cylinder can be calculated by means of Eqn (2.18):

$$\zeta_2(\sigma) \equiv \zeta^{in}(\sigma, \tau_2)$$

$$= C_0 + r_2 \sin \psi_2 \ln(2 \cosh \tau_2 - 2 \cos \sigma), \quad (3.5)$$

where the constant C_0 is determined by Eqn (2.33). The dependence of ζ_2 on σ means that the contact line is not horizontal. The inclination of the contact line can be characterized by the angle η defined as follows:

$$\tan \eta = \frac{1}{2r_2} [\zeta^{in}(\pi, \tau_2) - \zeta^{in}(0, \tau_2)] \quad (3.6)$$

By substituting from Eqn (2.18) into Eqn (3.6) one obtains

$$\tan \eta = \sin \psi_2 \ln \frac{1 + \exp(-\tau_2)}{1 - \exp(-\tau_2)} \quad (3.7)$$

In addition, from Eqn (2.5) one derives

$$\tau_2 = \ln\left(\frac{a}{r_2} + \sqrt{1 + \frac{a^2}{r_2^2}}\right) \quad (3.8)$$

As shown in Appendix B, when the separation between the cylinder and the wall is large enough ($r_2/s \ll 1$), the inclination angle of the contact line η is small compared with the meniscus slope angle ψ_2:

$$\frac{\tan \eta}{\sin \psi_2} \approx \frac{r_2}{s} \ll 1.$$

This result will be utilized below to calculate the capillary interaction between a sphere instead of cylinder and a wall.

The mean elevation, h_2, of the contact line $\zeta_2(\sigma)$ over the plane xy is

$$h_2 = \frac{1}{2\pi r_2} \oint_{C_2} \zeta_2 \, dl \tag{3.9}$$

where C_2 is the circumference, representing the projection of the contact line on the plane xy. Also, $dl = \sqrt{g_{\sigma\sigma}} \, d\sigma$, where $g_{\sigma\sigma}$ is a component of the respective metric tensor. After substituting the value of $g_{\sigma\sigma}$ given in Ref. [18] one obtains

$$h_2 = \frac{a}{\pi r_2} \int_0^\pi \frac{\zeta_2(\sigma) \, d\sigma}{\cosh \tau_2 - \cos \sigma} \tag{3.10}$$

Finally, by means of Eqns (2.19), (2.33), (3.5) and (3.10) one derives

$$h_2 = \frac{1}{q} \tan \psi_1 + r_2 \sin \psi_2$$

$$\times \left\{ \tau_2 + 2 \ln \left[\frac{1 - \exp(-2\tau_2)}{\gamma_e q a} \right] \right\} \quad (qa)^2 \ll 1 \tag{3.11}$$

Equation (3.11), together with Eqns (2.6) and (3.8), determines the dependence of h_2 on the distance s between the cylinder and the wall. Figure 4 illustrates the dependence of the mean elevation h_2 on the distance s between the cylinder and the wall for three different values of the cylinder radius r_2. As could be expected, h_2 increases with decrease of s or with increase of r_2. At large separations ($r_2 \ll s \ll q^{-1}$), an asymptotic expression for h_2 can
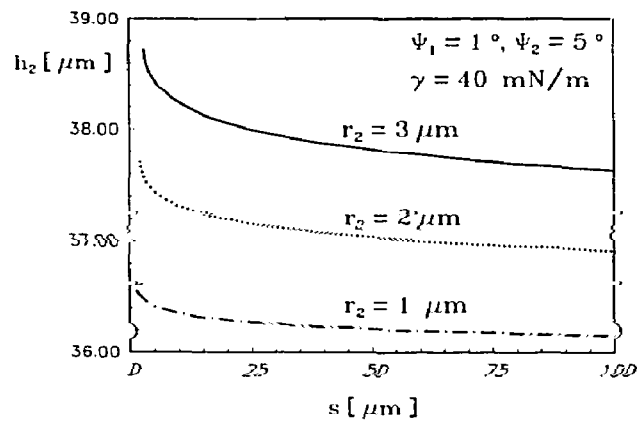

Fig. 4. Mean elevation of the cylinder contact line, h_2, vs the distance s between the cylinder and the wall for three different values of cylinder radius r_2.

be derived (see Appendix B):

$$h_2 \approx \frac{1}{q} \tan \psi_1 + r_2 \sin \psi_2 \left[\ln \left(\frac{2}{\gamma_e q r_2} \right) - \ln(\gamma_e q s) \right] \tag{3.11a}$$

The numerical calculations show that Eqns (3.11) and (3.11a) provide coincident results except in the case of small distances between the cylinder and the wall.

It should be noted that in the case of a single cylinder ($s \to \infty$, $a \to \infty$) the elevation of the contact line is given by the Derjaguin [21] formula:

$$h_{2\infty} = r_2 \sin \psi_2 \ln \frac{4}{\gamma_e q r_2 (1 + \cos \psi_2)}$$

$$(q r_2)^2 \ll 1 \tag{3.12}$$

Since Eqn (3.11) holds for $(qa)^2 \ll 1$, one cannot obtain Eqn (3.12) by setting $a \to \infty$ in Eqn (3.11).

Finally, it is worthwhile recalling that the asymptotic expressions for the slope of the meniscus and the contact lines derived above are valid when

$$(qa)^2 \ll 1 \qquad \sin^2 \psi_k \ll 1 \qquad k = 1, 2 \tag{3.13}$$

4. Capillary interaction between a vertical cylinder and a wall

The capillary force exerted on the cylinder or on the wall can be calculated by integrating the

meniscus interfacial tension along the contact line and the hydrostatic pressure through the wet surface of the respective body:

$$F^{(k)} = F^{(k\gamma)} + F^{(kp)} \qquad k = 1, 2 \tag{4.1}$$

where

$$F^{(k\gamma)} = \int_{L_k} \gamma \, \mathrm{d}l \qquad F^{(kp)} = -\int_{S_k} p \, \mathrm{d}S \tag{4.2}$$

where L_k and S_k ($k = 1, 2$) symbolize the respective contact line and wet surface, γ is the meniscus surface tension considered as a vector and p is the hydrostatic pressure. (We recall that $k = 1$ and $k = 2$ refer to the wall and the cylinder respectively.) It is worthwhile noting that $F^{(k)}$ is a force which is liable to direct measurement. As proven in Appendix A, $|F_x^{(1)}| = |F_x^{(2)}|$; here and subsequently the subscript x denotes the x-component of the respective force. In this respect one can say that the capillary forces obey Newton's third law. (Note, however, that in general $|F_x^{(1\gamma)}| \neq |F_x^{(2\gamma)}|$ and $|F_x^{(1p)}| \neq |F_x^{(2p)}|$.) Below we calculate independently $F_x^{(1)}$ and $F_x^{(2)}$, and compare the results. The coincidence between $|F_x^{(1)}|$ and $|F_x^{(2)}|$ would be an indication of the correctness of the asymptotic expressions for the meniscus shape derived above.

4.1 Capillary force exerted on the wall

As shown in Fig. 3 both the wet area of the wall and the shape of the contact line change when varying the distance between the cylinder and the wall. Since the surface of the wall is supposed to be infinite along the y axis, it is expedient to denote $F^{(1)}$ the increment of the capillary force exerted on the wall, which is due to the presence of the cylinder at some finite distance s from the wall. One can realize that in fact $F^{(1)}$ equals the net force exerted on the two sides of the plate depicted in Fig. 1. The only non-trivial component of $F^{(1)}$ is the x component because the x axis is directed from the wall towards the cylinder (Fig. 1).

The x component of $F^{(1\gamma)}$ reads

$$F_x^{(1\gamma)} = \gamma \cos \psi_1 \int_{-\infty}^{+\infty} \left(\frac{\mathrm{d}y}{\cos \theta} - \mathrm{d}y \right) \tag{4.3}$$

where the angle θ characterizes the running slope of the contact line:

$$\tan \theta = \frac{\mathrm{d}\zeta_1}{\mathrm{d}y} \tag{4.4}$$

Bearing in mind Eqns (2.7) and (4.4) one obtains

$$\frac{1}{\cos \theta} = \sqrt{1 + \tan^2 \theta} \approx 1 + \frac{1}{2}\left(\frac{\mathrm{d}\zeta_1}{\mathrm{d}y}\right)^2 \tag{4.5}$$

Also, in view of Eqn (3.13) one can set $\cos \psi_1 \approx 1$. Then Eqn (4.3) transforms to read

$$F_x^{(1\gamma)} = \gamma \int_0^\infty \left(\frac{\mathrm{d}\zeta_1}{\mathrm{d}y}\right)^2 \mathrm{d}y \tag{4.6}$$

According to Eqn (4.6), $F_x^{(1\gamma)}$ is always positive irrespective of the sign of angle ψ_2. From Eqn (3.1) one easily derives

$$\frac{\mathrm{d}\zeta_1}{\mathrm{d}y} = 2r_2 \sin \psi_2 \left[\frac{a^2}{y(y^2 + a^2)} - qK_1(qy)\right] \tag{4.7}$$

Equations (4.6) and (4.7) allow calculation of $F_x^{(1\gamma)}$ by means of numerical integration.

Below we proceed with the derivation of an expression for $F_x^{(1p)}$. The hydrostatic pressure in the two neighbouring phases is

$$p_Y = p_0 - \rho_Y gz \qquad Y = \mathrm{I}, \mathrm{II} \tag{4.8}$$

where $p_0 = \text{constant}$ is the pressure at the level $z = 0$ (see Fig. 1). Then the x component of $F^{(1p)}$ reads

$$F_x^{(1p)} = \int_{-\infty}^{+\infty} \mathrm{d}y \int_{\zeta_\infty}^{\zeta_1} \mathrm{d}z(p_{\mathrm{II}} - p_{\mathrm{I}})$$

$$= \Delta\rho g \int_0^\infty [\zeta_1^2(y) - \zeta_\infty^2] \, \mathrm{d}y \tag{4.9}$$

where Δp and ζ_α are defined by Eqns (2.9) and (3.2). Equation (4.9), along with Eqn (3.1), allows calculation of $F_x^{(1p)}$ by means of numerical integration.

4.2 Capillary force exerted on the cylinder

For the sake of convenience we make a special choice of the coordinate system (see Fig. 5). The z axis coincides with the axis of the cylinder. The plane $z = 0$ as usual coincides with the horizontal fluid interface far from the cylinder and wall. The x axis is directed from the cylinder towards the wall. The symmetry of the system implies that the y components of $F^{(2\gamma)}$ and $F^{(2p)}$ are equal to zero. That is why our task is reduced to a calculation of

$$F_x^{(2\gamma)} = e_x \cdot F^{(2\gamma)} \qquad \text{and} \qquad F_x^{(2p)} = e_x \cdot F^{(2p)}$$

$$\tag{4.10}$$

where e_x is the unit vector of the x axis. Because of the specific choice of the coordinate system, positive (negative) values of $F_x^{(k)}$ correspond to capillary attraction (repulsion) between the wall $(k = 1)$ and the cylinder $(k = 2)$. (Indeed, in both cases the x axes are oriented from the body under consideration towards the other body.)

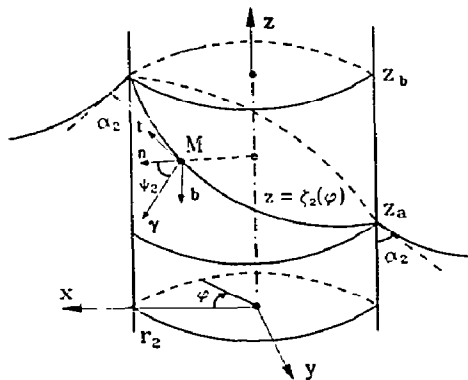Let $z = \zeta_2(\varphi)$ be the equation of the contact line with φ being the azimuthal angle in the plane xy (Fig. 5).

Fig. 5. Sketch of the contact line $z = \zeta_2(\varphi)$ on a vertical cylinder of radius r_2; γ is the interfacial tension and angle ψ_2 characterizes the meniscus slope at the contact line.

Then the linear element along the contact line is

$$dl = \chi \, d\varphi \qquad \chi = \left[r_2^2 + \left(\frac{d\zeta_2}{d\varphi} \right)^2 \right]^{1/2} \tag{4.11}$$

The vector of the running unit tangent to the contact line is

$$t = \frac{1}{\chi} \left(-r_2 \sin \varphi e_x + r_2 \cos \varphi e_y + \frac{d\zeta_2}{d\varphi} e_z \right) \tag{4.12}$$

(e_y and e_z are the unit vectors of the respective axes). Similarly the vector of the running unit normal to the cylindrical surface is

$$n = \cos \varphi e_x - \sin \varphi e_y \tag{4.13}$$

At a given point M of the contact line one can define the vector of the unit running binormal as follows:

$$b = n \times t \tag{4.14}$$

Since the vector of the interfacial tension γ belongs to the plane formed by the vectors n and b, one can write

$$\gamma = \gamma(\sin \psi_2 b + \cos \psi_2 n) \tag{4.15}$$

(see Fig. 5). Then by substituting from Eqns (4.12)–(4.14) into Eqn (4.15) one obtains

$$\gamma_x \equiv e_x \cdot \gamma = \gamma \left(\cos \varphi \cos \psi_2 - \frac{1}{\chi} \frac{d\zeta_2}{d\varphi} \sin \varphi \sin \psi_2 \right)$$

$$\tag{4.16}$$

From Eqns (4.2), (4.10), (4.11) and (4.16) one derives

$$F_x^{(2\gamma)} = -2\gamma \sin \psi_2 \int\limits_0^\pi \frac{d\zeta_2}{d\varphi} \sin \varphi \, d\varphi + \Delta F_x^{(2)} \tag{4.17}$$

where

$$\Delta F_x^{(2)} = \gamma \cos \psi_2 \int\limits_0^{2\pi} \chi \cos \varphi \, d\varphi$$

$$\approx \gamma \cos \psi_2 \frac{1}{r_2} \int\limits_0^\pi \left(\frac{d\zeta_2}{d\varphi} \right)^2 \cos \varphi \, d\varphi$$

Above we derived an expression for calculating ζ_2 as a function of σ (see Eqn (3.5)). Therefore it is more convenient to use σ for parameterization of the contact line, instead of the azimuthal angle φ. From Eqns (2.2) and (2.4) one can obtain the connection between the two parameters, φ and σ:

$$\cos \varphi = \frac{1 - \cosh \tau_2 \cos \sigma}{\cosh \tau_2 - \cos \sigma}$$

$$0 \leqslant \varphi \leqslant \pi \qquad 0 \leqslant \sigma \leqslant \pi \qquad (4.18)$$

where τ_2 is given by Eqn (3.8). A combination of Eqns (4.17) and (4.18) yields

$$F_x^{(2\gamma)} = 2\gamma \sin \psi_2 \sinh \tau_2$$

$$\times \int_0^\pi \frac{\mathrm{d}\zeta_2}{\mathrm{d}\sigma} \frac{\sin \sigma \, \mathrm{d}\sigma}{\cosh \tau_2 - \cos \sigma} + \Delta F_x^{(2)} \qquad (4.19)$$

From Eqn (2.18) one obtains

$$\frac{\mathrm{d}\zeta_2}{\mathrm{d}\sigma} = \frac{r_2 \sin \psi_2 \sin \sigma}{\cosh \tau_2 - \cos \sigma} \qquad (4.20)$$

By using the identity

$$\int_0^\pi \frac{\sin^2 \sigma \, \mathrm{d}\sigma}{(\cosh \tau - \cos \sigma)^2} = \frac{\pi \exp(-\tau)}{\sinh \tau} \qquad (4.21)$$

from Eqns (4.19) and (4.20) one derives

$$F_x^{(2\gamma)} = 2\pi r_2 \gamma \sin^2 \psi_2 \exp(-\tau_2) + \Delta F_x^{(2)} \qquad (4.22)$$

Finally, by substituting from Eqns (2.6) and (3.8) into Eqn (4.22) one obtains the explicit dependence of $F_x^{(2\gamma)}$ on the distance s:

$$F_x^{(2\gamma)} = \frac{2\pi r_2^2 \gamma \sin^2 \psi_2}{s + \sqrt{s^2 - r_2^2}} + \Delta F_x^{(2)} \qquad (4.23)$$

where

$$\Delta F_x^{(2)} = \frac{\gamma}{a} \cos \psi_2 \int_0^\pi \left(\frac{\mathrm{d}\zeta_2}{\mathrm{d}\sigma}\right)^2 (1 - \cosh \tau_2 \cos \sigma) \, \mathrm{d}\sigma$$

The last integral can be calculated numerically after substituting the expression for $\mathrm{d}\zeta_2/\mathrm{d}\sigma$ from Eqn (4.20).

A simple asymptotic formula for $F_x^{(2\gamma)}$ can be obtained in the case of large separation between the cylinder and the wall $(r_2/s \ll 1)$ (see Appendix B). The result reads

$$F_x^{(2\gamma)} \approx \pi \gamma r_2^2 \sin^2 \psi_2 \frac{1}{s} \qquad r_2 \ll s \ll q^{-1} \qquad (4.23a)$$

Equation (4.23a) shows that the capillary force decays very slowly with the distance s, i.e. $F_x^{(2\gamma)}$ is very long-range.

Below we proceed with the derivation of an expression for $F_x^{(2p)}$. Let z_a and z_b be the coordinates of the highest and of the lowest point of the contact line (Fig. 5). The parameter S_2 in Eqn (4.2) can be chosen to be that part of the cylinder surface existing between the planes $z = z_a$ and $z = z_b$. Besides, one has to substitute in Eqn (4.2) (for $k = 2$) the following expression for p:

$$p = \begin{cases} p_I & \text{for} & z < \zeta_2(\varphi) \\ p_{II} & \text{for} & z > \zeta_2(\varphi) \end{cases} \qquad (4.24)$$

Accordingly, from Eqns (4.2), (4.10) and (4.24) one obtains

$$F_x^{(2p)} = -\int_{-\pi}^\pi \mathrm{d}\varphi \, r_2 \cos \varphi \left[\int_{z_a}^{\zeta_2} p_I \, \mathrm{d}z + \int_{\zeta_2}^{z_b} p_{II} \, \mathrm{d}z \right] \qquad (4.25)$$

A substitution from Eqns (4.8) and (4.24) into Eqn (4.25) yields

$$F_x^{(2p)} = \Delta \rho g r_2 \int_0^\pi \zeta_2^2 \cos \varphi \, \mathrm{d}\varphi \qquad (4.26)$$

As mentioned earlier, it is more convenient to use σ as an integration variable in Eqn (4.26). By differentiating Eqn (4.18) one obtains

$$\frac{\mathrm{d}\varphi}{\mathrm{d}\sigma} = -\frac{\sinh \tau_2}{\cosh \tau_2 - \cos \sigma} \qquad (4.27)$$

Finally, Eqns (2.5), (4.18), (4.26) and (4.27) yield

$$F_x^{(2p)} = \Delta\rho g a \int_0^\infty \frac{1 - \cosh \tau_2 \cos \sigma}{(\cosh \tau_2 - \cos \sigma)^2} \zeta_2^2(\sigma)\, d\sigma \qquad (4.28)$$

where $\zeta_2(\sigma)$ is given by Eqn (3.5). Equation (4.28) allows calculation of $F_x^{(2p)}$ by means of numerical integration.

The series expansion of Eqn (4.28) leads to the following asymptotic formula for $F_x^{(2p)}$ (see Appendix B):

$$F_x^{(2p)} \approx \pi\gamma(qr_2)^2 h_2 r_2 \sin \psi_2 \cdot \frac{1}{s} \qquad r_2 \ll s \ll q^{-1}$$

$$(4.28a)$$

The comparison between Eqns (4.28a) and (4.23a) shows that $F_x^{(2p)}/F_x^{(2\gamma)} \approx q^2 r_2 h_2/\sin \psi_2$ in the range of validity of the asymptotic expressions used. When $\tan \psi_1$ is of the order of $\sin \psi_2$, in keeping with Eqns (3.11a) and (3.13) one obtains $F_x^{(2p)}/F_x^{(2\gamma)} \approx qr_2 \ll 1$.

4.3 Numerical results and discussion

Our aim below is to compare the capillary forces $F_x^{(kp)}$ ($k = 1, 2$) due to the hydrostatic pressure with the capillary forces $F_x^{(k\gamma)}$ due to the interfacial tension, as well as to compare the total capillary forces $F_x^{(1)}$ with $F_x^{(2)}$. It should be noted that the numerical values of the parameters used below obey Eqn (3.13), which determines the range of validity of our analytical expressions. Figure 6 represents data for $F_x^{(1p)}$ and $F_x^{(2p)}$ calculated by means of Eqns (4.9) and (4.28) respectively. The values of the parameters used are $\gamma = 40$ mN m^{-1}, $r_2 = 1$ μm, $\psi_1 = 1°$, $\psi_2 = \pm 5°$, $\Delta\rho = 1$ g cm^{-3}. One can see that $F_x^{(1p)}$ is much larger than $F_x^{(2p)}$. In addition, when the angles ψ_1 and ψ_2 have the same sign, both $F_x^{(1p)}$ and $F_x^{(2p)}$ are positive and correspond to attraction between the cylinder and the wall. On the other hand, when ψ_1 and ψ_2 are of different sign, both $F_x^{(1p)}$ and $F_x^{(2p)}$ are negative and correspond to repulsion between the cylinder and the wall.

In contrast with $F_x^{(kp)}$, $F_x^{(k\gamma)}$ can only be positive, i.e. the force due to the surface tension in all cases leads to attraction between the cylinder and the wall. Moreover $F_x^{(1\gamma)} \approx F_x^{(2\gamma)}$ as could be expected, because $F_x^{(k\gamma)} \gg F_x^{(kp)}$ (see Figs 6 and 7).

Table 1 contains data for the total capillary force $F_x^{(k)} = F_x^{(kp)} + F_x^{(k\gamma)}$, $k = 1, 2$. Since $F_x^{(1)}$ and $F_x^{(2)}$ must be equal (see Appendix A) the comparison between the calculated values of these two forces provides a test for the self-consistency of the asymptotic expressions for the meniscus shape derived above. In particular, $F_x^{(1)}$ is calculated by means of Eqns (4.6) and (4.9) whereas $F_x^{(2)}$ is calculated by means of Eqns (4.23) and (4.28). Both $F_x^{(1)}$ and $F_x^{(2)}$ turn out to be positive and coincide
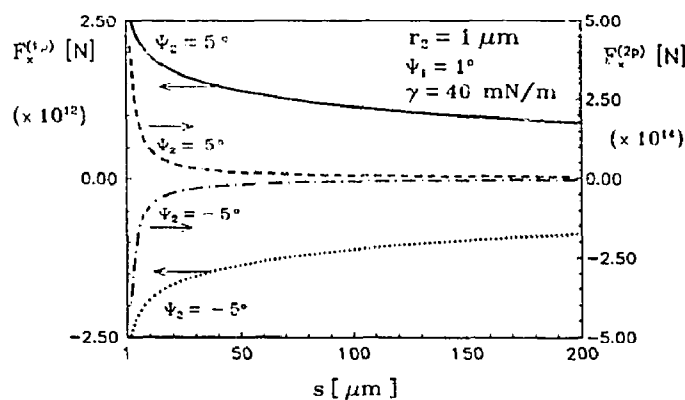

Fig. 6. Plot of the capillary force $F_x^{(kp)}$ due to the hydrostatic pressure vs the distance s between the wall ($k = 1$) and the cylinder ($k = 2$).
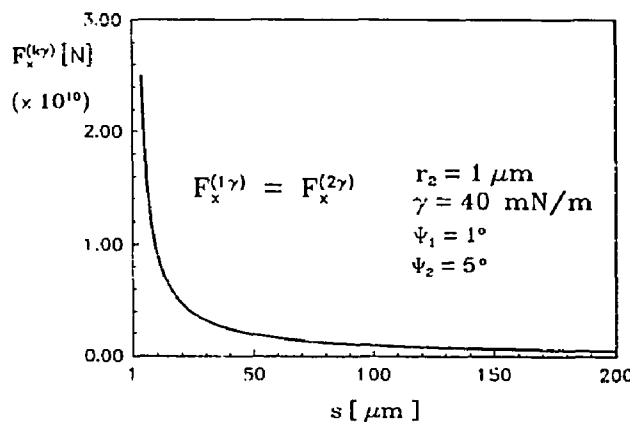

Fig. 7. Plot of the capillary force $F_x^{(k\gamma)}$ due to the meniscus interfacial tension vs the distance s between the cylinder and the wall.

TABLE 1

Comparison between $F_x^{(1)}$ and $F_x^{(2)}$ for different values of the distance s between the cylinder and the wall for $r_2 = 1$ μm; $\psi_1 = 1°$, $\psi_2 = 5°$, $\gamma = 40$ mN m^{-1}

s(μm)	$F_x^{(1)}$(N)	$F_x^{(2)}$(N)
10	$9.64 \cdot 10^{-11}$	$9.60 \cdot 10^{-11}$
20	$4.81 \cdot 10^{-11}$	$4.78 \cdot 10^{-11}$
30	$3.20 \cdot 10^{-11}$	$3.18 \cdot 10^{-11}$
40	$2.39 \cdot 10^{-11}$	$2.39 \cdot 10^{-11}$
50	$1.91 \cdot 10^{-11}$	$1.91 \cdot 10^{-11}$
60	$1.59 \cdot 10^{-11}$	$1.59 \cdot 10^{-11}$
70	$1.36 \cdot 10^{-11}$	$1.36 \cdot 10^{-11}$
80	$1.18 \cdot 10^{-11}$	$1.19 \cdot 10^{-11}$
90	$1.04 \cdot 10^{-11}$	$1.06 \cdot 10^{-11}$
100	$9.37 \cdot 10^{-12}$	$9.55 \cdot 10^{-12}$
110	$8.48 \cdot 10^{-12}$	$8.68 \cdot 10^{-12}$
120	$7.74 \cdot 10^{-12}$	$7.96 \cdot 10^{-12}$
130	$7.10 \cdot 10^{-12}$	$7.34 \cdot 10^{-12}$
140	$6.55 \cdot 10^{-12}$	$6.82 \cdot 10^{-12}$
150	$6.10 \cdot 10^{-12}$	$6.36 \cdot 10^{-12}$

with the absolute value of the horizontal projection of the capillary force. Table 1 shows that the calculated values of $F_x^{(1)}$ and $F_x^{(2)}$ are practically equal. The more pronounced differences for large values of the distance s are connected with the condition $(qa)^2 \ll 1$, which determines the range of validity of our asymptotic expressions. The latter condition can be violated for very large values of the distance s (see Eqn (2.6)). It should be noted that the forces $F_x^{(2\gamma)}$ and $F_x^{(2p)}$ calculated by means of the asymptotic expressions, Eqns (4.23a) and (4.28a), practically coincide with the results from the general expressions, Eqns (4.23) and (4.28), except for small distances between the cylinder and the wall.

It might seem that the forces of capillary interaction between a cylinder of micron radius and a wall are too small to have any physical importance. The following estimate can answer this question.

The quantity

$$\Delta W_2(s) = - \int_{r_2}^{s} F_x^{(2\gamma)} \, ds \qquad (4.29)$$

represents the work done by the capillary force to bring the cylinder from a distance s from the wall

to the position of close contact ($s = r_2$). Since both terms in the right-hand side of Eqn (4.23) are positive, by substituting from Eqn (4.23) into Eqn (4.29) one can derive

$$|\Delta W_2(s)| > \int_{r_2}^{s} \frac{2\pi r_2^2 \gamma \sin^2 \psi_2}{s + \sqrt{s^2 - r_2^2}} \, ds$$

$$= \pi \gamma \sin^2 \psi_2 \left[s^2 - r_2^2 - s\sqrt{s^2 - r_2^2} \right.$$

$$\left. + r_2^2 \ln \left(\frac{s}{r_2} + \sqrt{\frac{s^2}{r_2^2} - 1} \right) \right] \qquad (4.30)$$

For $r_2 \ll s \ll q^{-1}$, Eqn (4.30) yields

$$|\Delta W_2(s)| > \pi \gamma \sin^2 \psi_2 r_2^2 \left[\ln \left(\frac{2s}{r_2} \right) - \frac{1}{2} \right] \qquad (4.31)$$

With $\gamma = 40$ mN m^{-1}, $\psi_2 = 5°$, $r_2 = 1$ μm and $s = 10r_2$ from Eqn (4.31) one obtains $|\Delta W_2| > 2.4 \cdot 10^{-15}$ J. This value is much larger than the thermal energy $kT \approx 10^{-21}$ J. Hence the capillary attraction is able to produce strong attachment of a microparticle to the wall. Indeed, as shown in the next section, Eqn (4.23) is applicable not only to cylinders but also to spherical particles.

5. Capillary interactions between a sphere and a wall

Let us consider a flat vertical wall and a flat horizontal plate, which is covered with a liquid layer (phase I) (see Fig. 8). In addition, let us consider a spherical particle which is put on the plate and is partially immersed in the liquid layer. It is supposed that far from the sphere and the wall the liquid layer has uniform thickness l_0. As usual, the coordinate plane xy is chosen to coincide with the horizontal fluid interface far from the wall.

We again restrict our considerations to the case of a small slope of the meniscus surface ($\sin^2 \psi_k \ll 1$, $k = 1, 2$; Fig. 8) and to a small deviation of the particle contact line from the horizontal position (see the discussion after Eqn (3.8)). Then the horizontal projection of the particle contact line can
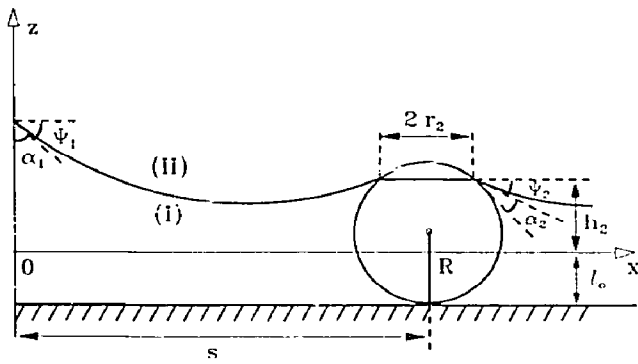
Fig. 8. Sketch of the capillary meniscus formed around a spherical particle which is situated at a distance s from a vertical wall. The sphere is partially immersed in a liquid layer whose thickness is equal to l_0 for $x \to \infty$. R and r_2 are the radii of the particle and of the three-phase contact line; α_1 and α_2 are the contact angles at the wall and the particle surface respectively.

be treated approximately as a circumference of radius r_2. In contrast with the case of a vertical cylinder considered above, in this case r_2 and ψ_2 depend on the distance s between the particle and the wall (Fig. 8). This dependence can be determined in the following way.

Let R be the radius of the spherical particle. From the equation of the spherical surface one can derive

$$r_2(h_2) = [(l_0 + h_2)(2R - l_0 - h_2)]^{1/2} \tag{5.1}$$

where h_2 is the mean elevation of the particle contact line over the flat horizontal surface far from the wall (Fig. 8). In addition, simple geometrical considerations yield

$$\psi_2(h_2) = \arcsin \frac{r_2(h_2)}{R} - \alpha_2 \tag{5.2}$$

where α_2 is the corresponding three-phase contact angle. Besides, at given values of s and ψ_1 Eqns (2.6), (3.8) and (3.11) determine h_2 as a function of r_2 and ψ_2:

$$h_2 = h_2[r_2(h_2), \psi_2(h_2)] \tag{5.3}$$

For each given distance s one can solve numerically Eqn (5.3) along with Eqns (5.1) and (5.2) to calculate h_2, r_2, ψ_2 and a. With the parameter values thus calculated one can determine the menis-

cus profile from Eqn (2.35), as well as the shape of the contact lines from Eqns (3.1) and (3.5). Then Eqns (4.3), (4.6), (4.23) and (4.28) allow calculation of the capillary forces $F_x^{(k,p)}$ and $F_x^{(k,p)}$, $k = 1, 2$.

The applicability of Eqn (4.28) for calculating $F_x^{(2,p)}$ needs some discussion. Indeed, the horizontal projection of the force exerted on an element ds_s from the surface of the spherical particle is $p \cos \theta \times ds_s = p \, ds_c$ (see Fig. 9). Here $ds_c = (ds_s) \cos \theta$ is the area of the orthogonal projection of ds_s on the surface of the respective cylinder (z_a and z_b are the same as in Fig. 5). Hence the integral of the pressure taken through the spherical belt (between z_a and z_b) can be approximately replaced by the integral through the respective belt from the surface of the cylinder. In other words, Eqn (4.26) and its corollary, Eqn (4.28), can also be used in the case of a spherical particle.

As an illustration, Fig. 10 represents the plot of $F_x^{(k)}$ vs the distance s (see Eqn (4.2)) for a spherical particle of radius $R = 1$ μm. The values of the other parameters are $\psi_1 = 0.01°$, $q^{-1} = 0.2$ cm and $l_0 = 0.5$ μm. The two curves correspond to two different values of the contact angle: $\alpha_2 = 1°$ and $\alpha_2 = 25°$. It turns out that $F_x^{(1)}$ and $F_x^{(2)}$ coincide again, as they should. Their values are positive and correspond to attraction between the particle and the wall.

The fact that the capillary force between a small particle and a vertical wall can be only attractive,
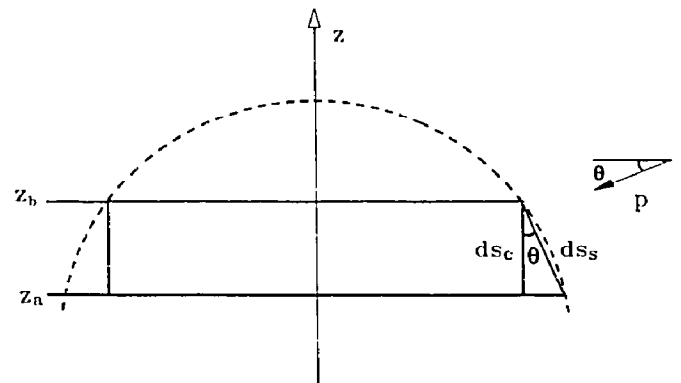

Fig. 9. Cross-section of a spherical particle. The pressure p is directed normally to the spherical surface element ds_s; ds_c is the projection of ds_s on the vertical cylindrical surface.
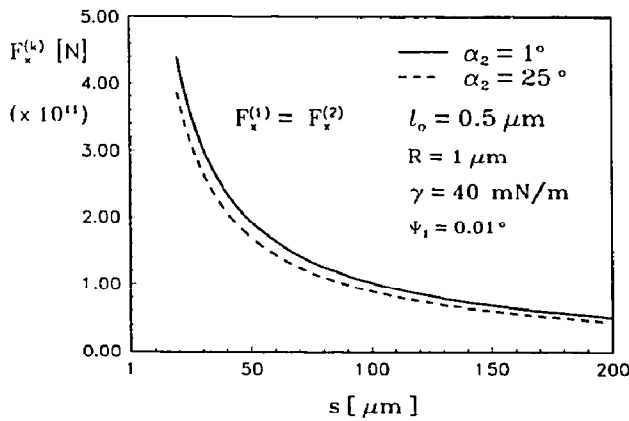
Fig. 10. Plot of the total capillary force $F_x^{(k)}$ due to interaction between a spherical particle and a wall vs the distance s for two different values of the particle three-phase contact angle α_2.
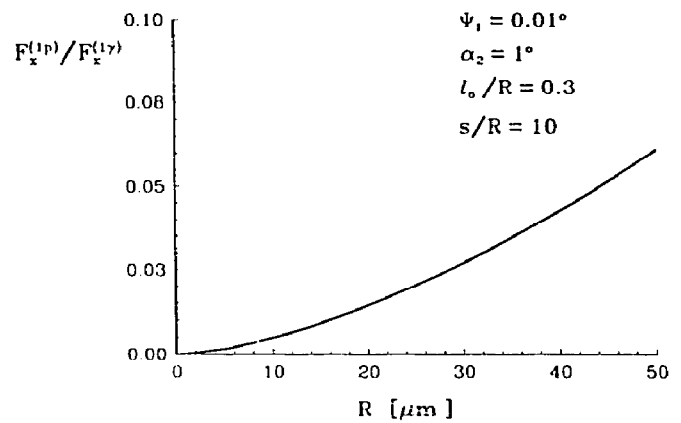

Fig. 11. Plot of $F_x^{(1p)}/F_x^{(1\gamma)}$ vs particle radius R for $s/R = 10$ and $l_0/R = 0.3$.

irrespective of the sign of angle ψ_2 (see Fig. 8), needs special discussion. It is known that a repulsive capillary meniscus interaction can exist between two particles when one of them forms a convex meniscus and the other one a concave meniscus (see for example Refs [14,16]). In our case, however, the geometry of the system is somewhat different. Indeed, since $qr_2 \ll 1$, the particle does not "feel" the slope of the meniscus created by the wall. This circumstance is reflected by Eqns (4.7) and (4.20) which show that the slope of the two contact lines does not depend on the meniscus slope at the wall, ψ_1. Moreover, Figs 2(a) and 2(b) demonstrate that for both positive ψ_2 (convex meniscus) and negative ψ_2 (concave meniscus) the length of the contact line on the wall is increased in comparison with the horizontal contact line for $s \to \infty$. However, this increase in the contact line length gives rise to a positive capillary force $F_x^{(1\gamma)}$ (see Eqns (4.3) and (4.6)). Moreover, for small particles, $F_x^{(1\gamma)} \gg F_x^{(1p)}$ and $F_x^{(1\gamma)} \approx F_x^{(1)}$. Therefore the total capillary force $F_x^{(1)}$ exerted on the wall must be positive. The same is true for the force $F_x^{(2)}$ exerted on the particle, which is to be equal to $F_x^{(1)}$ (see Appendix A).

The situation can change for larger particles when $F_x^{(1p)}$ can be comparable in magnitude with $F_x^{(1\gamma)}$. Figure 11 represents the dependence of the ratio $F_x^{(1p)}/F_x^{(1\gamma)}$ vs the particle radius R for $l_0/R =$

0.3 and $s/R = 50$. One can see that the contribution of the hydrostatic pressure to the total capillary force increases with the increase in the particle radius.

6. Concluding remarks

The main finding of the present paper is that capillary forces play a dominant role for colloidal particles attached to a liquid interface in the vicinity of a vertical wall (or a particle aggregate of much larger size). This conclusion is based on the following results.

(i) An analytical expression for the shape of the capillary meniscus formed around a vertical cylinder near a vertical flat wall is derived (see Fig. 1 and Eqn (2.35)). It allows calculation of the shape of the three-phase contact lines (see Eqns (3.1) and (3.5)).

(ii) An equation for the mean elevation h_2 of the cylinder contact line is also derived. It is a counterpart of the known Derjaguin equation for "a meniscus on a needle" (see Eqns (3.11) and (3.12)).

(iii) The expressions for the case of a vertical cylinder near a wall can also be applied for the case of a spherical particle near a wall (see Fig. 8).

(iv) It turns out that the horizontal projections of the force $F^{(1)}$ exerted on the wall and of the force $F^{(2)}$ exerted on the particle (cylinder) must be equal (see Appendix A).

(v) Each of the forces $F^{(1)}$ and $F^{(2)}$ is a super-position of a force $F^{(kp)}$, due to the hydrostatic pressure p, and a force $F^{(k\gamma)}$, $k = 1, 2$, due to the meniscus interfacial tension γ.

(vi) Depending on the contact angles of the wall and cylinder (particle), $F^{(kp)}$ can be attractive or repulsive (see Fig. 6). In contrast, $F^{(k\gamma)}$ in all cases leads to attraction between the cylinder (particle) and the wall (see Fig. 7).

(vii) Simple asymptotic expressions for $F_x^{(k\gamma)}$ and $F_x^{(kp)}$ are derived for large distances between the cylinder and the wall (see Eqns (4.23a) and (4.28a)).

The forces $F^{(1)}$ and $F^{(2)}$ are liable to direct measurement. The meniscus shape can be also determined experimentally by means of different interferometric techniques (see for example Ref. [22]). Hence there are various ways to verify experimentally the present theoretical results.

The basic analytical expression for the meniscus shape derived in this paper, Eqn (2.35), represents a zeroth-order term of an asymptotic expansion for small meniscus slope and small particles (see Eqn (3.13)). That is why, in the case of liquid–gas interfaces, the expressions derived in this paper are valid for particle (cylinder) radii of the order of 100 μm or smaller. (In the case of liquid–liquid interfaces the capillary length q^{-1} is larger and the range of validity of the theory can be wider.) Fortunately, this is the range of size of microparticles and colloidal particles. As discussed in the text, the energy of capillary attraction turns out to be larger than the thermal energy kT even with micron-size particles. Therefore we believe our results can be useful for interpreting experimental data about two-dimensional coagulation and microparticle ordering at a liquid–fluid interface near a vertical wall. When the thickness l_0 of the liquid layer (see Fig. 8) is small enough, the action of the disjoining pressure should also be taken into account (see for example Refs [15] and [23]).

Acknowledgement

References

1 D.F. Gerson, J.E. Zajic and M.D. Ouchi, in M. Tomlinson (Ed.), Chemistry for Energy, ACS Symp. Ser. ' . American Chemical Society, Washington, DC, 1979, p. 77.
2 J.D. Henry, M.E. Prudich and K.P. Vaidyanathan, Sep. Purif. Methods, 8 (1979) 81.
3 K. Hinsch, J. Colloid Interface Sci., 92 (1983) 243.
4 C. Camoin, J.F. Rouseil, R. Faure and R. Blanc, Europhys. Lett., 3 (1987) 449.
5 P. Pieranski, Phys. Rev. Lett., 45 (1980) 569.
6 G.Y. Onoda, Phys. Rev. Lett., 55 (1985) 226.
7 S. Hayashi, Y. Kumamoto, T. Suzuki and T. Hirai, J. Colloid Interface Sci., 144 (1991) 538.
8 H. Yoshimura, S. Endo, M. Matsumoto, K. Nagayama and Y. Kagawa, J. Biochem., 106 (1989) 958.
9 H. Yoshimura, M. Matsumoto, S. Endo and K. Nagayama, Ultramicroscopy, 32 (1990) 265.
10 L. Haggerty, B.H. Watson, M.A. Barteau and A.M. Lenhoff, J. Vac. Sci. Technol., B9 (1991) 1219.
11 M.M. Nicolson, Proc. Cambridge Philos. Soc., 45 (1949) 288.
12 D.Y.C. Chan, J.D. Henry and L.R. White, J. Colloid Interface Sci., 79 (1981) 410.
13 W.A. Gifford and L.E. Scriven, Chem. Eng. Sci., 26 (1971) 287.
14 M.A. Fortes, Can. J. Chem., 60 (1982) 2889.
15 P.A. Kralchevsky, V.N. Paunov, I.B. Ivanov and K. Nagayama, J. Colloid Interface Sci., 151 (1992) 79.
16 P.A. Kralchevsky, V.N. Paunov, N.D. Denkov, I.B. Ivanov and K. Nagayama, J. Colloid Interface Sci., in press.
17 R. Finn, Equilibrium Capillary Surfaces, Springer Verlag, New York, 1986.
18 G.A. Korn and T.M. Korn, Mathematical Handbook, McGraw-Hill, New York, 1968.
19 A.H. Nayfeh, Perturbation Methods, Wiley, New York, 1973.
20 A.J. McConnel, Application of Tensor Analysis, Dover, New York, 1957.
21 B. Derjaguin, Dokl. Akad. Nauk SSSR, 51 (1946) 517.
22 A.S. Dimitrov, P.A. Kralchevsky, A.D. Nikolov and D.T. Wasan, Colloids Surfaces, 47 (1990) 299.
23 P.A. Kralchevsky and I.B. Ivanov, Chem. Phys. Lett., 121 (1985) 116.

Appendix A: The capillary forces and Newton's third law

Let $F_{\text{II}}^{(k)}$ ($k = 1, 2$) be the projection of the capillary force $F^{(k)}$ on the horizontal coordinate plane

xy. The choice of the coordinate system is the same as in Fig. 1. Our aim here is to prove that the horizontal projections of capillary forces exerted on the wall ($k = 1$) and on the cylinder (or spherical particle, $k = 2$) have the same magnitude, but opposite sign, i.e. that

$$F_{\text{II}}^{(2)} = -F_{\text{II}}^{(1)} \qquad \text{(A1)}$$

Equation (A1) can be considered as a counterpart of Newton's third law. It is demonstrated that Eqn (A1) holds because the shape of the capillary meniscus surface satisfies the Laplace equation along with the condition for constancy of the three-phase contact angles. We consider again the case where the slope of the meniscus surface is small (cf. Eqn (2.7)). However, our derivation is not limited to small values of the radius r_2 or to small distances, s, between the wall and the cylinder (particle) (see Figs 1 and 8).

Let us first consider the capillary force exerted on the cylinder (particle). From Eqns (4.1) and (4.2) one obtains

$$F_{\text{II}}^{(2)} = \oint_{L_2} \mathrm{d}l\, \gamma_{\text{II}} + \oint_{C_2} \mathrm{d}l\, \mu \int_{z_n}^{z_b} \mathrm{d}z\, p \qquad \text{(A2)}$$

where L_2 denotes the respective contact line and C_2 is its projection on the horizontal plane xy; μ is a running unit vector normal to the contour C_2 directed inwards; z_a and z_b are the same as in Eqn (4.25); γ_{II} is a vector representing the horizontal projection of the interfacial tension γ.

From Eqns (4.12)–(4.15) one can derive

$$\gamma_{\text{II}} = -\gamma \left(e_\sigma \frac{\mathrm{d}\zeta_2}{\mathrm{d}l} \sin \psi_2 + e_\tau \cos \psi_2 \right) \qquad \text{(A3)}$$

where e_σ and e_τ are the running unit vectors tangential to the σ and τ lines in bipolar coordinates (cf. Eqn (2.2)). In our case, e_σ and e_τ represent also units tangent and normal to the contour C_2. In particular

$$\oint_{C_2} \mathrm{d}l\, e_\tau = 0 \qquad \text{(A4)}$$

$$\frac{\mathrm{d}\zeta_2}{\mathrm{d}l} = -\frac{1}{\lambda} \frac{\partial \zeta}{\partial \sigma}\Big|_{\tau = \tau_2} \qquad \lambda = \frac{a}{\cosh \tau_2 - \cos \sigma} \qquad \text{(A5)}$$

see also Ref. [18]. In addition

$$\oint_{L_2} \mathrm{d}l\, \gamma_{\text{II}} = \oint_{C_2} \frac{\mathrm{d}l}{\cos \theta} \gamma_{\text{II}} = \oint_{C_2} \mathrm{d}l\, \gamma_{\text{II}} \left[1 + \left(\frac{\mathrm{d}\zeta_2}{\mathrm{d}l} \right)^2 \right]^{1/2} \qquad \text{(A6)}$$

where the angle θ characterizes the running slope of the contact line L_2. By expanding the square root in Eqn (A6) and by using Eqns (A3) and (A4) one obtains

$$\oint_{L_2} \mathrm{d}l\, \gamma_{\text{II}} = -\gamma \oint_{C_2} \mathrm{d}l \left[e_\sigma \frac{\mathrm{d}\zeta_2}{\mathrm{d}l} \sin \psi_2 + e_\tau \frac{1}{2} \left(\frac{\mathrm{d}\zeta_2}{\mathrm{d}l} \right)^2 \right] \qquad \text{(A7)}$$

where the higher-order terms with respect to the slope are neglected (see Eqn (2.7)). Then, having in mind the constancy of angle ψ_2 from Eqns (2.14), (A4), (A5) and (A7), one derives

$$\oint_{L_2} \mathrm{d}l\, \gamma_{\text{II}} = \gamma \oint_{C_2} \mathrm{d}l \left\{ \left(e_\sigma \frac{1}{\lambda} \frac{\partial \zeta}{\partial \sigma} + e_\tau \frac{1}{\lambda} \frac{\partial \zeta}{\partial \tau} \right) \sin \psi_2 \right.$$
$$\left. - e_\tau \frac{1}{2\lambda^2} \left[\left(\frac{\partial \zeta}{\partial \sigma} \right)^2 + \left(\frac{\partial \zeta}{\partial \tau} \right)^2 \right] \right\}$$

The last equation can be transformed to read

$$\oint_{L_2} \mathrm{d}l\, \gamma_{\text{II}} = \gamma \oint_{C_2} \mathrm{d}l \left[e_\tau \cdot (\nabla \zeta) \nabla \zeta - \frac{1}{2} e_\tau (\nabla \zeta) \cdot \nabla \zeta \right] \qquad \text{(A8)}$$

where ∇ is the gradient operator in the plane xy and the relation $\sin \psi_2 = e_\tau \cdot \nabla \zeta (\tau = \tau_2)$ was used. However, similarly to Eqn (4.26) one can derive

$$\oint_{C_2} \mathrm{d}l\, \mu \int_{z_n}^{z_b} \mathrm{d}z\, p = -\Delta \rho g \oint_{C_2} \mathrm{d}l\, \mu \frac{1}{2} \zeta^2 \qquad \text{(A9)}$$

Equations (2.9), (A2), (A8) and (A9) yield

$$F_{\text{II}}^{(2)} = \gamma \oint_{C_2} \mathrm{d}l\, \mu \cdot \left\{ (\nabla \zeta) \nabla \zeta - \frac{1}{2} U [(\nabla \zeta) \cdot \nabla \zeta + q^2 \zeta^2] \right\}$$

$$\text{(A10)}$$

where $\mu = e_z$ and U is the idem factor (the unit tensor) in the plane xy. It should be noted that contour C_2 in Eqn (A10) is oriented clockwise.

Our aim below is to prove that a counterpart of Eqn (A10) holds for the capillary force $F_{\text{II}}^{(1)}$ exerted on the vertical plate (see Fig. 1):

$$F_{\text{II}}^{(1)} = \gamma \oint_{C_1} \mathrm{d}l\, \boldsymbol{\mu} \cdot \left\{ (\boldsymbol{\nabla}\zeta)\boldsymbol{\nabla}\zeta - \frac{1}{2} U[(\boldsymbol{\nabla}\zeta)\cdot\boldsymbol{\nabla}\zeta + q^2\zeta^2] \right\}$$

(A11)

where C_1 is a degenerate contour consisting of two straight lines parallel to the y axis representing the orthogonal projections of the left-hand and right-hand side contact lines on the horizontal plane xy. It is supposed that, similarly to contour C_2, contour C_1 is oriented inwards. Then Eqn (A11) can be represented in the form

$$F_{\text{II}}^{(1)} = I_1 + I_2 + I_3$$

(A12)

where

$$I_1 = \gamma \int_{-\infty}^{+\infty} \mathrm{d}y\, \boldsymbol{e}_x \cdot [(\boldsymbol{\nabla}\zeta)\boldsymbol{\nabla}\zeta|_{x=-d} - (\boldsymbol{\nabla}\zeta)\cdot\boldsymbol{\nabla}\zeta|_{x=0}]$$

(A13)

$$I_2 = -\frac{\gamma}{2}\boldsymbol{e}_x \int_{-\infty}^{+\infty} \mathrm{d}y\, [(\boldsymbol{\nabla}\zeta)\cdot\boldsymbol{\nabla}\zeta|_{x=-d} - (\boldsymbol{\nabla}\zeta)\cdot\boldsymbol{\nabla}\zeta|_{x=0}]$$

(A14)

$$I_3 = -\frac{\gamma}{2}q^2\boldsymbol{e}_x \int_{-\infty}^{+\infty} \mathrm{d}y\, [\zeta^2|_{x=-d} - \zeta^2|_{x=0}]$$

(A15)

where $\boldsymbol{e}_x$ is the unit vector of the x axis; $x = -d$ and $x = 0$ are the x coordinates of the left-hand and right-hand side contact lines on the plate (cf. Fig. 1). Having in mind that

$$\boldsymbol{e}_x \cdot \boldsymbol{\nabla}\zeta|_{x=-d} = -\boldsymbol{e}_x \cdot \boldsymbol{\nabla}\zeta|_{x=0} = \tan\psi_1$$

$$\boldsymbol{e}_y \cdot \boldsymbol{\nabla}\zeta|_{x=-d} = 0$$

(A16)

one can easily derive

$$I_1 = \gamma \tan\psi_1 \int_{-\infty}^{+\infty} \mathrm{d}y (\boldsymbol{\nabla}\zeta|_{x=-d} + \boldsymbol{\nabla}\zeta|_{x=0})$$

$$= \gamma \tan\psi_1\, \boldsymbol{e}_y \int_{-\infty}^{+\infty} \mathrm{d}y \left. \frac{\partial\zeta}{\partial y} \right|_{x=0}$$

Since $\zeta(x = 0) = \zeta_1(y)$ is an even function of y (see Eqn (3.1) and Fig. 3), one obtains

$$I_1 = 0$$

(A17)

Besides

$$(\boldsymbol{\nabla}\zeta)\cdot\boldsymbol{\nabla}\zeta|_{x=-d} = \tan^2\psi_1$$

$$(\boldsymbol{\nabla}\zeta)\cdot\boldsymbol{\nabla}\zeta|_{x=0} = \tan^2\psi_1 + \left(\frac{\mathrm{d}\zeta_1}{\mathrm{d}y}\right)^2$$

$$\zeta|_{x=-d} = \zeta_x, \qquad \zeta|_{x=0} = \zeta_1(y)$$

Then Eqns (A14) and (A15) reduce to

$$I_2 = \gamma\,\boldsymbol{e}_x \int_0^{+\infty} \mathrm{d}y \left(\frac{\mathrm{d}\zeta_1}{\mathrm{d}y}\right)^2$$

(A18)

$$I_3 = \gamma q^2\,\boldsymbol{e}_x \int_0^{+\infty} \mathrm{d}y\, [\zeta_1^2(y) - \zeta_x^2]$$

(A19)

From Eqns (2.9), (4.6), (4.9), (A12) and (A17)–(A19) one obtains

$$F_{\text{II}}^{(1)} = \boldsymbol{e}_x[F_x^{(1\,\gamma)} + F_x^{(1\,p)}]$$

(A20)

as it must be. In fact, Eqn (A20) proves the validity of Eqn (A11). As known, ζ tends exponentially to zero far away from the plate (see for example Eqn (2.27)). Then by means of Eqns (A10) and (A11) and by using the Green's theorem (see for example Ref. [20]) one obtains

$$F_{\text{II}}^{(1)} + F_{\text{II}}^{(2)} = -\gamma \int_{S_m} \mathrm{d}s \left\{ \boldsymbol{\nabla} \cdot [(\boldsymbol{\nabla}\zeta)\boldsymbol{\nabla}\zeta] \right.$$

$$\left. - \frac{1}{2}\boldsymbol{\nabla}[(\boldsymbol{\nabla}\zeta)\cdot\boldsymbol{\nabla}\zeta + q^2\zeta^2] \right\}$$

(A21)

where S_m is the orthogonal projection of the meniscus surface on the plane xy. By using the Laplace equation (Eqn (2.8)) one can derive

$$\nabla \cdot [(\nabla \zeta)\nabla \zeta] = \frac{1}{2} \nabla [q^2 \zeta^2 + (\nabla \zeta) \cdot (\nabla \zeta)] \tag{A22}$$

The substitution from Eqn (A22) into Eqn (A21) leads to the sought for relation, Eqn (A1), representing a counterpart of Newton's third law.

Appendix B: Capillary meniscus interaction at a large separation between the cylinder and the wall

When the distance between the cylinder and the wall is large compared with the cylinder radius, simple asymptotic formulae for the capillary interaction energy and force can be obtained by using appropriate series expansions of the general expressions. We consider the case where the quantity

$$c = \frac{r_2}{s} \ll 1 \tag{B1}$$

is a small parameter with r_2 and s being repectively the cylinder radius and the distance between the axis of the cylinder and the wall (see Fig. 1). In terms of the small parameter c, Eqn (2.6) can be written in the form

$$a = s\sqrt{1 - c^2} \approx s[1 + O(c^2)] \tag{B2}$$

From Eqn (3.8) one obtains

$$\tau_2 \approx \ln \left\{ \frac{2}{c} [1 + O(c^2)] \right\} \tag{B3}$$

$$\frac{1}{2} \exp \tau_2 \approx \sinh \tau_2 \approx \cosh \tau_2 \approx \frac{1}{c} [1 + O(c^2)] \tag{B4}$$

By substituting the expressions (B3) and (B4) into Eqn (3.11) we derive the following asymptotic formula for the mean elevation of the three-phase contact line around the cylinder:

$$h_2 \approx \frac{1}{q} \tan \psi_1 + r_2 \sin \psi_2 \ln \left(\frac{2}{\gamma_c q s} \right)$$
$$- r_2 \sin \psi_2 \ln(\gamma_c q s)[1 + O(c)] \tag{B5}$$

If we are interested in the angular dependence of the elevation of the contact line around the cylinder, we have to keep the leading term containing the angle σ in the series expansion of Eqn (3.5).

Equation (B6), together with Eqns (3.6), (3.7) and (B1), reveals that the inclination of the contact line, characterized by means of the angle η, is small compared with the slope angle ψ_2 of the meniscus at the cylinder surface:

$$\frac{\tan \eta}{\sin \psi_2} \approx \frac{\eta}{\psi_2} \approx \frac{r_2}{s} [1 + O(c^2)] \ll 1 \tag{B6}$$

Asymptotic expressions for the capillary forces acting on the cylinder can be found by expanding Eqns (4.23) and (4.28):

$$F_x^{(2\eta)} \approx \pi \gamma r_2^2 \sin^2 \psi_2 \frac{1}{s} [1 + O(c^2)] \tag{B7}$$

$$F_x^{(2p)} \approx \pi \gamma (q r_2)^2 h_2 r_2 \sin \psi_2 \frac{1}{s} [1 + O(c)] \tag{B8}$$

where h_2 is given by Eqn (B5). The comparison between Eqns (B7) and (B8) shows that $F_x^{(2p)} \ll F_x^{(2\eta)}$ because $(q r_2)^2 \ll 1$. It is interesting to note that the leading term in the asymptotics of the capillary force $F_x^{(2\eta)}$, given by Eqn (B7), coincides with the respective asymptotic expression for the capillary force acting between two similar cylinders of radius r_2 and meniscus slope angle ψ_2, separated at a distance $L = 2s$ (see Ref. [16]).

As shown in Section 4, for $r_2 \ll s \ll q^{-1}$, the energy ΔW_2 of interaction between the cylinder and the wall can be expressed approximately by means of Eqn (4.31):

$$|\Delta W_2(s)| \approx \pi \gamma r_2^2 \sin^2 \psi_2 \ln s + \text{constant} \tag{B9}$$

In fact, the latter expression can be obtained by integration of the capillary force acting between the cylinders (see Eqn (B7)). The constant of integration in Eqn (B9) depends on the choice of a reference state of zero interaction energy.

The numerical calculations show that Eqns (B5)–(B9), although quite simple, describe very well the capillary interactions except in the case of a small separation between the cylinder and a wall.

138

V.N. Paunov et al. Colloids Surfaces 67 (1992) 119–138

One should also keep in mind that the asymptotic formulae, as well as the general expressions are restricted to small slopes of the meniscus profile (sin $\psi_k \ll 1$, $k = 1, 2$) and to not very large distances ($qs \ll 1$), i.e. the approximate expressions (B2)–(B9) are strictly applicable for separations s satisfying the relationship

$$r_2 \ll s \ll q^{-1} \qquad (\text{B10})$$

This region corresponds to the case of capillary interactions between colloidal particles. If r_2 and ψ_2 are known, the expressions (B5)–(B9) can also be used for describing the interaction between a sphere and a wall. To estimate r_2 and ψ_2 for the case of a sphere, the asymptotic expressions, Eqns (B5)–(B9), can be used, along with the geometrical relationships, Eqns (5.1) and (5.2).